1   **Sphingosine kinases promote Ebola virus infection and can be targeted to inhibit**

2   **filoviruses, coronaviruses, and arenaviruses using late endocytic trafficking to enter cells**

3

4   Corina M. Stewart[1,2,3], Yuxia Bo[1,2,3], Kathy Fu[1,2,3], Mable Chan[4,5], Robert Kozak[4,#], Kim Yang-

5   Ping Apperley[6,7], Geneviève Laroche[1,2,3], André Beauchemin[6,7], Gary Kobinger[8], Darwyn

6   Kobasa[4,5], Marceline Côté[1,2,3,6]*

7

8   [1] Department of Biochemistry, Microbiology and Immunology, University of Ottawa, Ottawa,

9   Canada

10   [2] Ottawa Institute of Systems Biology, University of Ottawa, Ottawa, Canada

11   [3] Centre for Infection, Immunity, and Inflammation, University of Ottawa, , Ottawa, Canada

12   [4] Special Pathogens Program, National Microbiology Laboratory, Public Health Agency of

13   Canada, Winnipeg, Canada

14   [5] Department of Infectious Diseases and Medical Microbiology, University of Manitoba,

15   Winnipeg, Canada

16   [6] Center for Catalysis Research and Innovation, University of Ottawa, Ottawa, Canada

17   [7] Department of Chemistry and Biomolecular Sciences, University of Ottawa, Ottawa, Canada

18   [8] Galveston National Laboratory, Department of Microbiology & Immunology, University of

19   Texas Medical Branch, Galveston, TX 77550, USA.

20   # Present address: Sunnybrook Health Sciences Center, Toronto, Canada

21   * Corresponding author

22   Email: marceline.cote@uottawa.ca (MC)

23   **Abstract**

24   Entry of enveloped viruses in host cells requires the fusion of the viral and host cell

25   membranes, a process that is facilitated by viral fusion proteins protruding from the viral

26   envelope. For fusion, viral fusion proteins need to be triggered by host factors and for some

27   viruses, such as Ebola virus (EBOV) and Lassa fever virus, this event occurs inside endosomes

28   and/or lysosomes. Consequently, these 'late-penetrating viruses' must be internalized and

29   delivered to entry-conducive intracellular vesicles. Because endocytosis and vesicular trafficking

30   are tightly regulated cellular processes, late penetrating viruses also depend on specific host

31   factors, such as signaling molecules, for efficient viral delivery to the site of fusion, suggesting

32   that these could be targeted for antiviral therapy. In this study, we investigated a role for

33   sphingosine kinases (SKs) in viral entry and found that chemical inhibition of sphingosine kinase

34   1 (SK1) and/or SK2 and knockdown of SK1 or SK2, inhibited entry of EBOV into host cells.

35   Mechanistically, inhibition of SK1 and/or SK2 prevented EBOV from reaching late-endosomes

36   and lysosomes that are positive for the EBOV receptor, Niemann Pick C1 (NPC1). Furthermore,

37   we present evidence that suggests the trafficking defect caused by SK1/2 inhibition occurs

38   independently of S1P signaling through cell-surface S1PRs. Lastly, we found that chemical

39   inhibition of SKs prevents entry of other late-penetrating viruses, including arenaviruses and

40   coronaviruses, in addition to inhibiting infection by replication competent EBOV and SARS-

41   CoV-2 in Huh7.5 cells. In sum, our results highlight an important role played by SKs in

42   endocytic trafficking which can be targeted to inhibit entry of late-penetrating viruses. SK

43   inhibitors could serve as a starting point for the development of broad-spectrum antiviral

44   therapeutics.

45

Introduction

To deliver the viral genome into host cells, enveloped viruses require the fusion between the viral and cellular membranes. This process is mediated by viral fusion proteins that protrude from the viral envelope and undergo a series of conformational changes triggered by interactions with host factors and/or environmental cues such as acidic pH. For Ebola virus (EBOV), the causative agent of outbreaks of severe hemorrhagic fevers in humans, its fusion protein, the viral glycoprotein (GP), requires cleavage by low pH-dependent cathepsin proteases and interaction with the late endosomal/lysosomal Niemann-Pick C1 protein (NPC1) (1-5). The strict late endosomal/lysosomal localization of the EBOV GP triggering factors results in a need for a multistep viral entry process involving attachment, internalization, and endosomal trafficking. Attachment of EBOV to the host cell is mediated by interactions of GP to cell surface carbohydrate binding proteins such as C-type lectins, and/or by binding of phosphatidylserine (PS) on the viral envelope to cell surface PS receptors such as Tim-1 or Axl (6-8). Once attached to the cell surface, internalization via macropinocytosis or phagocytosis is triggered and is followed by endosomal trafficking to late endosomes and lysosomes where viral fusion occurs (2, 3, 9-14).

Many host proteins have been identified to be important for endosomal trafficking of EBOV, such as the small GTPase Rab7, the homotypic fusion and protein sorting (HOPS) complex, the UV Radiation Resistance Associated (UVRAG) protein, and the PIKfyve-ArPIKfyve-Sac3 trafficking complex (10, 15, 16). In addition, studies have shown that EBOV particles can stimulate signaling cascades such as the Akt/PI3K pathway, the latter being required for EBOV trafficking to NPC1 (16-19). In a previous study, we screened a kinase inhibitor library to identify other signaling pathways important for EBOV entry (18). We identified 35 compounds that inhibited EBOV entry, including inhibitors of receptor tyrosine

70   kinases (RTKs), AMP-activated protein kinase (AMPK), and Akt, some of which have

71   previously been shown to be important for virus internalization and trafficking (17-20).

72   Additionally, inhibitors of sphingosine kinase 1 (SK1) and sphingosine-1-phosphate G-protein

73   coupled receptors (S1PR) were also identified, suggesting a role for the SK-S1PR axis in EBOV

74   GP-mediated entry (18). Interestingly, Imre and colleagues reported that a sphingosine kinase 1

75   activator or the overexpression of SK1 reduced EBOV-GP mediated entry, further suggesting a

76   role for SK1 in EBOV entry, although the mechanism remains to be elucidated (21).

77   Sphingosine kinases 1 and 2 (SK1/2) catalyze the phosphorylation of sphingosine to

78   sphingosine-1-phosphate (S1P). Despite their polypeptide sequence similarity, SK1 and 2 appear

79   to have distinct physiological functions; generally, SK1 promotes cell survival and proliferation

80   while SK2 is pro-apoptotic (22). S1P has both extracellular and intracellular targets.

81   Extracellular S1P activates signaling pathways through a family of five S1P GPCRs ($S1PR_{1-5}$),

82   while intracellular S1P has been shown to modulate the activity of multiple enzymes including p-

83   21 activated kinase 1 (Pak1), which is an important regulator of macropinocytosis (23-25). In

84   addition, recent studies have also demonstrated a link between SK1, levels of sphingosine, and

85   regulation of endocytic membrane trafficking (26, 27). Their putative roles in macropinocytosis

86   and trafficking indicate that SK1 and SK2 may be entry host factors for EBOV and potential

87   targets for antiviral therapy.

88   Viruses, such as EBOV, that enter cells via late endosomes or lysosomes are termed late

89   penetrating viruses. Other examples of such viruses are Lassa fever virus (LFV) and severe acute

90   respiratory syndrome coronaviruses -1 and -2 (SARS-CoV-1 and SARS-CoV-2). LFV entry

91   requires low pH and interaction with the lysosomal-associated membrane protein 1 (LAMP-1)

92   (28-31). Therefore, similarly to EBOV, LFV must be internalized and undergo endo-lysosomal

93   trafficking to reach entry-conducive intracellular vesicles (32). As for SARS-CoV-1 and -2, the

94   cellular localization of fusion depends on the expression and activity of cell surface proteases

95   that are required for priming and/or triggering (33-36). More specifically, SARS-CoV-1 can

96   utilize surface serine proteases, while SARS-CoV-2 is more promiscuous in its protease usage,

97   having been shown to utilize both surface serine proteases and metalloproteases for entry at the

98   cell surface (33-37). In the absence of surface or extracellular proteases, the entry of SARS CoV-

99   1 and -2 depends on internalization and trafficking to late endosomes containing cathepsin L (36,

100 38-40). Although the triggering factors are different for each of these viruses, one commonality

101 is a need for endosomal trafficking in host cells, raising the possibility that they may share the

102 use of host trafficking factors (41).

103   Here, we investigated the role of sphingosine kinases in cellular entry of EBOV and other

104 late penetrating viruses. We found that treatment with sphingosine kinase inhibitors and

105 knockdown of sphingosine kinase 1 and 2 reduced EBOV growth and/or EBOV GP-mediated

106 entry. More specifically, the sphingosine kinase inhibitors blocked trafficking of EBOV viral-

107 like particles (VLPs) to NPC1 independently of S1P signaling through S1PRs. Lastly, we found

108 that treatment with the SK inhibitors reduced entry of other late penetrating viruses and blocked

109 cathepsin-dependent infection of SARS CoV-2. Our results suggest that SKs play a critical role

110 in regulating endosomal trafficking and that inhibition of SK activity results in trafficking

111 defects that prevent late-penetrating viruses from reaching entry-conducive compartments.

112

113

114

115

Results

Sphingosine kinase inhibitors reduce entry of EBOV VLPs

Previously, we screened a library of kinase inhibitors using murine leukemia virus (MLV) pseudotypes to identify signaling pathways required for EBOV GP-mediated entry (18). Among the hits were two compounds, PF-543 and FTY-720 (fingolimod, 2-amino-2-(2-(4-octylphenyl)-ethyl)-1,3-propanediol), that interfere with the SK/S1PR signaling axis, suggesting that this pathway plays an important role in EBOV entry. PF-543 is a SK1 and SK2 competitive inhibitor, while FTY-720 (fingolimod, 2-amino-2-(2-(4-octylphenyl)-ethyl)-1,3-propanediol) is a structural analog of sphingosine that becomes phosphorylated by SK1 and SK2, albeit more efficiently by SK2, and thus can inhibit the SKs (42, 43). We therefore sought to investigate the possible role of the SK/S1PR signaling pathway in EBOV entry by validating and characterizing the antiviral activity of these inhibitors and that of SK1-I, which is a sphingosine analogue that is highly specific to SK1 over SK2 and was not present in the screening library (44). To confirm the antiviral activity of PF-543, FTY-720, and SK1-I, we used filoviral-like particles (VLPs) generated by the co-expression of the EBOV nucleoprotein (NP), matrix protein (VP40) fused to a β-lactamase (βlam) reporter, and the glycoprotein of interest (45). We found that treatment with all three inhibitors reduced entry of VLPs harbouring EBOV GP (Figure 1A-C). Importantly, the inhibitors had no effect on entry of VLPs harbouring the vesicular stomatitis virus (VSV) G protein, indicating that the compounds target an EBOV GP-mediated entry step (Figure 1A-C).
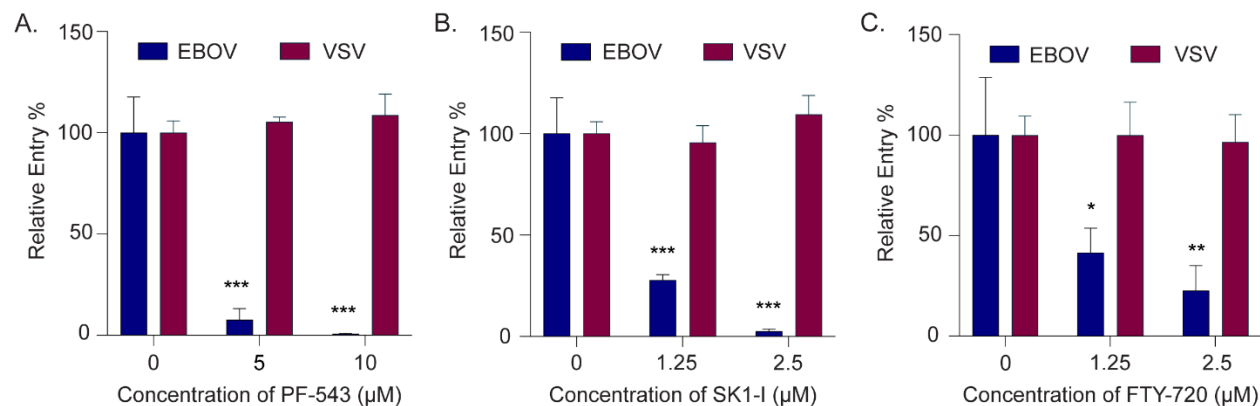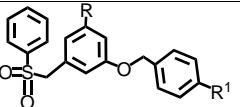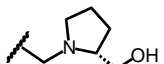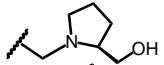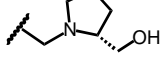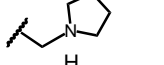
Figure 1. Sphingosine kinase inhibitors block EBOV GP-mediate entry

Entry of βlam VLPs harbouring EBOV GP or VSV G in HT1080 cells treated with (A) PF-543, (B) SK1-I, (C) FTY-720, or vehicle (DMSO, 0.1%) at the indicated concentrations. Relative entry % was determined by measuring the percentage of inhibitor-treated cells with cleaved βlam substrate (CCF2) compared to vehicle-treated cells. Results are expressed as mean ± s.d. of triplicates and are representative of three experiments. Variance for each virus-inhibitor treatment was analyzed by one-way ANOVA, followed by Dunnett's multiple comparisons test to determine significance. * $p < 0.05$, ** $p < 0.01$, *** $p < 0.001$.
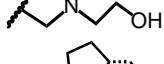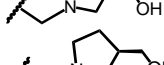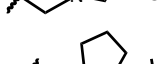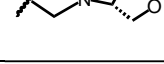
Given their common therapeutic targets, the antiviral activity of PF-543, SK1-I and FTY720 support a role for SKs in EBOV entry. To further confirm this, we synthesized PF-543 analogs with various level of inhibitory activity against SK1, SK2, or both, using a previously published structure-activity-relationship study of the compound (see supporting information for details) (46). The analogs were analyzed for *in vitro* inhibition of SK1 and SK2 activity and for antiviral activity (Table 1, Figure 2). We found that the most potent antiviral compounds were those that strongly inhibited SK1 activity, suggesting that inhibition of EBOV GP-mediated entry is associated with SK1 inhibitory activity (Figure 2). In addition, antiviral activity was

155   severely compromised for compounds that poorly inhibited SK1 activity (>40% residual activity

156   at 1 μM of inhibitor) (Table 1, Figure 2). Lastly, the only compound that was more specific for

157   SK2 and less active against SK1 (Compound 39, SK1 activity: ~52.6%, SK2 activity: 16.3%)

158   had no antiviral activity (Table 1). Although more work needs to be done to validate the *in*

159   *cellulo* SK inhibitory activity of these compounds, this panel of inhibitors and the antiviral

160   activity of SK1-I and FTY-720 strongly support a role for SKs, especially SK1, in EBOV GP-

161   mediated entry.

162

163   ***Table 1. Activity of PF-543 derivative on SK1/2 and EBOV entry***

		R	SK1 activity* (% ± std)	SK2 activity **(% ± std)	Relative entry *** (% ± std)
16		CH$_3$	5.4 ± 13.3	28.1 ± 43.0	0.1 ± 0.3
18		CH$_3$	35.6 ± 54.6	62.3 ± 18.6	2.3 ± 2.2
19		H	0.3 ± 4.4	0.1 ± 6.0	13.3 ± 6.8
35		CH$_3$	22.5 ± 41.3	130.3 ± 41.0	0.6 ± 1.0
36		CH$_3$	52.2 ± 38.5	87.5 ± 42.1	56.1 ± 17.0
37		CH$_3$	43.0 ± 19.6	61.8 ± 44.9	118.5 ±. 26.0
38		CH$_3$	46.1 ± 35.2	86.3 ± 30.1	109.5 ± 19.1
39		CH$_3$	52.6 ± 33.3	16.3 ± 4.1	107.5 ± 6.0

164
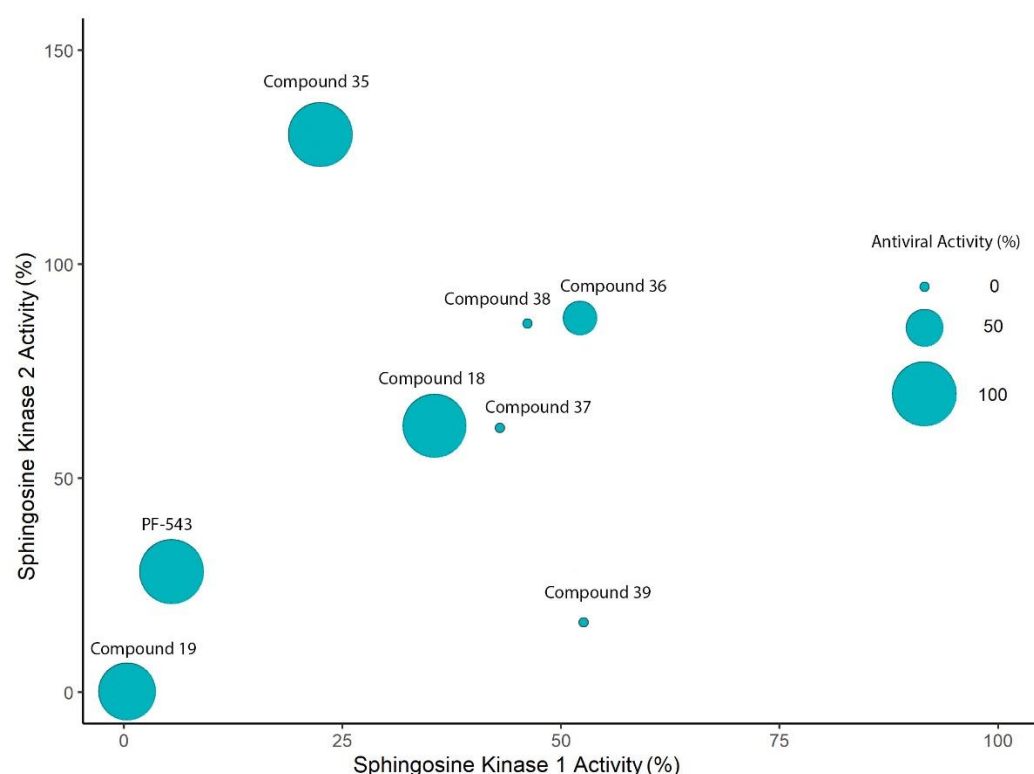
Figure 2. Study of the relationship between antiviral and SK1/2 inhibitory activities using derivatives of PF-543

SK1 and SK2 activity was measured *in vitro* by measuring fluorescence after incubation of PF-543 derivatives (1 µM) or vehicle (DMSO, 0.1%) with SK reaction buffers containing light-sensitive NBD-sphingosine. Percent SK activity was calculated in comparison to vehicle, which represents 100% activity. In parallel, antiviral activity was determined by treating HT1080 cells with the PF-543 derivatives (10 µM) or vehicle (0.1%) and transducing them with MLV pseudotypes encoding LacZ and harbouring EBOV GP. Relative antiviral activity (%) was determined by quantifying LacZ positive inhibitor treated cells compared to vehicle treated cells. Mean SK1 activity (x-axis) and SK2 activity (y-axis) was plotted as a bubble chart using R studio with the size of the bubble representing mean antiviral activity.

177   ***Knockdown of sphingosine kinase 1 and 2 reduces EBOV GP-mediated entry***

178   To directly assess a role for SKs, we targeted SK1 and SK2 using Dicer-Substrate Short

179   Interfering RNAs (DsiRNAs). SK1 or SK2 targeting DsiRNAs, or a non-targeting negative

180   control, were transfected in HT1080 cells. Immunoblot analysis confirmed that SK1 and SK2

181   expression was substantially knocked down when the respective DsiRNA was transfected

182   (Figure 3A). VLPs harboring EBOV GP or VSV-G were then used to measure entry (Figure 3B).

183   While knockdown of SK1 or SK2 did not interfere with VSV-G-mediated entry, a decrease in

184   entry of EBOV VLPs was observed. Interestingly, although expression of each SK was

185   undetectable when cells were transfected with their respective targeting DsiRNA, SK2

186   knockdown had a slightly greater inhibitory effect on EBOV entry (Figure 3B). To test whether

187   they play redundant roles in viral entry, we tried to perform double knockdown. Unfortunately,

188   viability of the cells was severely compromised (data not shown). Nevertheless, these results

189   suggest that both SK1/2 play a role in infection, providing even further evidence that EBOV GP-

190   mediated entry requires SK1 and/or SK2 activity.

191

192

193
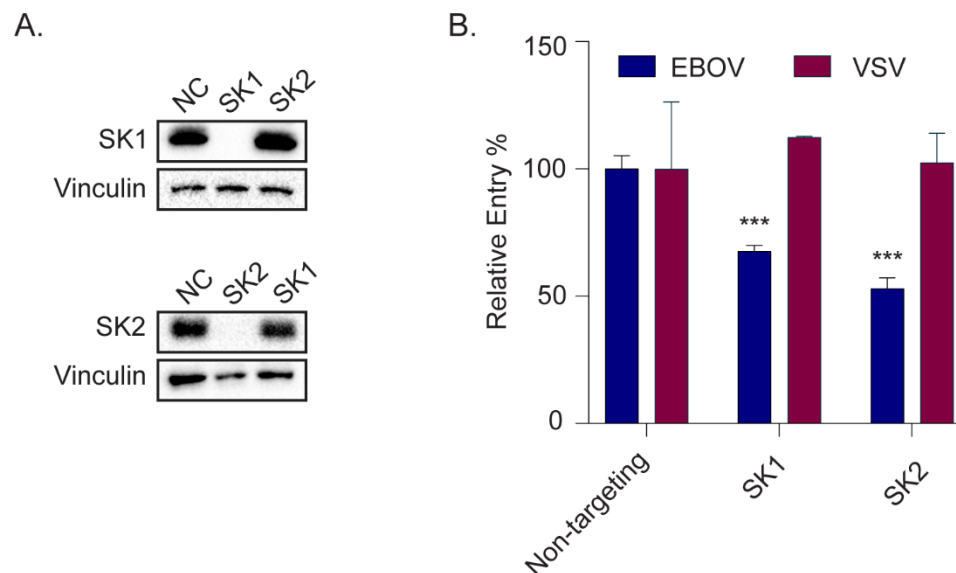
Figure 3. SK1/2 knockdown blocks entry of EBOV in HT1080

HT1080 cells transfected with nontargeting control dsiRNA (NC: negative control) or dsiRNA targeting SK1 or SK2 were either (A) lysed and expression of SK1 or SK2 (upper) and Vinculin (lower) detected by immunoblot, or (B) infected with βlam VLPs harbouring EBOV GP or VSV G. Relative entry % was determined by measuring the percentage of inhibitor-treated cells with cleaved βlam substrate (CCF2) compared to vehicle-treated cells. Results are expressed as mean ± s.d. of triplicates and are representative of three experiments. Variance was analyzed by one-way ANOVA, followed by Dunnett's multiple comparisons test to determine significance. *** $p < 0.001$.

PF-543 blocks EBOV growth

We next sought to confirm that SK1/2 activity is required for replicative EBOV infection. Given that our data indicate that both SK1 and SK2 are involved in entry, we chose to investigate the effect of PF-543, which inhibits both SKs, on infection by replication-competent EBOV.

209   Vero cells were infected with Green Fluorescent Protein (GFP)-expressing replicative EBOV in

210   the presence or absence of PF-543 and growth was assessed by measuring GFP fluorescence. We

211   found that PF-543 significantly inhibited replicative EBOV at 5µM and completely prevented it

212   at 10µM (Figure 4 AB). These results further support a role of SKs in EBOV infection and

213   suggest that they are potential targets for antiviral therapy.

214
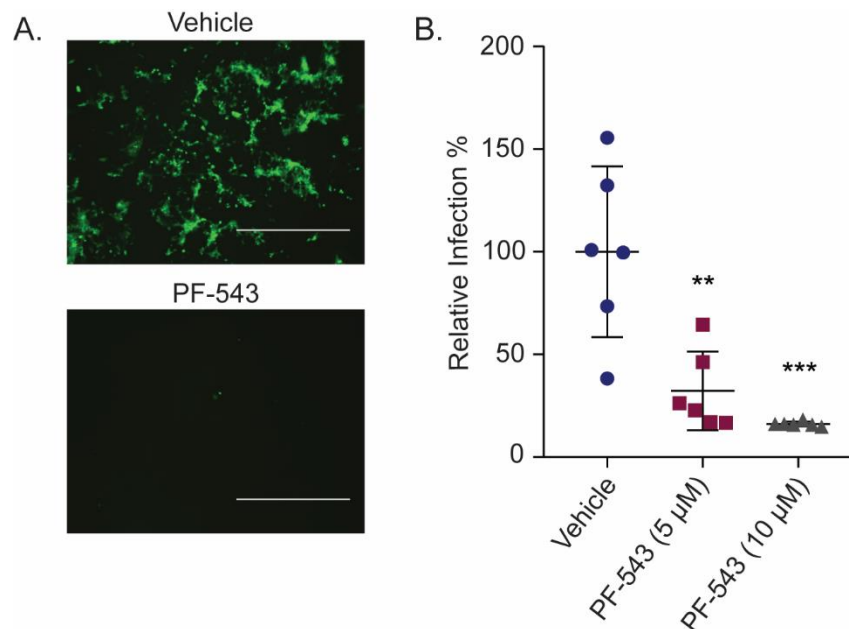
Figure 4. PF-543 blocks infection of replication-competent EBOV

216   Infection of Vero cells with replication-competent EBOV expressing GFP and treated with

217   vehicle or PF-543. Images in (A) were acquired for vehicle or PF-543 (5 µM) treated wells,

218   bar=1mm. Relative infection % in (B) was determined by measuring mean GFP fluorescence

219   intensity for PF-543 treated cells compared to vehicle alone. Results are expressed as mean ± s.d.

220   of three experiments. Variance was analyzed by one-way ANOVA, followed by Dunnett's

221   multiple comparisons test to determine significance. * $p < 0.05$, ** $p < 0.01$, *** $p < 0.001$.

222

223   *Sphingosine kinase inhibitors do not interfere with EBOV attachment and internalization*

224   EBOV entry begins with attachment of the viral particle to the cell surface, which is

225   mediated by multiple cellular attachment factors, followed by virion internalization via a

226   macropinocytosis-like mechanism (10). To further elucidate the role of sphingosine kinases in

227   EBOV entry, we first assessed whether the SK inhibitors reduced attachment of EBOV using

228   EBOV VLPs containing VP40 fused to GFP. We exposed inhibitor-treated cells to EBOV VLPs

229   at 4 °C to only allow for virion attachment and assessed the resulting VLP fluorescence by flow

230   cytometry. We found that none of the inhibitor treatments resulted in a reduction in VLP

231   fluorescence, indicating that SK inhibitors do not significantly block attachment of EBOV VLPs

232   (Figure 5A).

233   To assess if the SK inhibitors blocked macropinocytic uptake of EBOV, we allowed virus

234   internalization at 37 °C following the 4 °C attachment step. As controls, some samples were kept

235   at 4˚C throughout the experiment to ensure that internalization could not occur, and some

236   samples were incubated with 5-(*N*-Ethyl-*N*-isopropyl)amiloride (EIPA), a known

237   macropinocytosis inhibitor (Figure 5B) (47). We found that while PF-543 had a modest effect on

238   internalization of fluorescent EBOV VLPs, the effect was not nearly as pronounced as that of

239   EIPA (Figure 5B). Notably, SK1-I and FTY720 had no effect on EBOV VLP internalization

240   (Figure 5B). Taken together, these results suggested that SK activity is required at an entry step

241   after attachment and internalization.

242
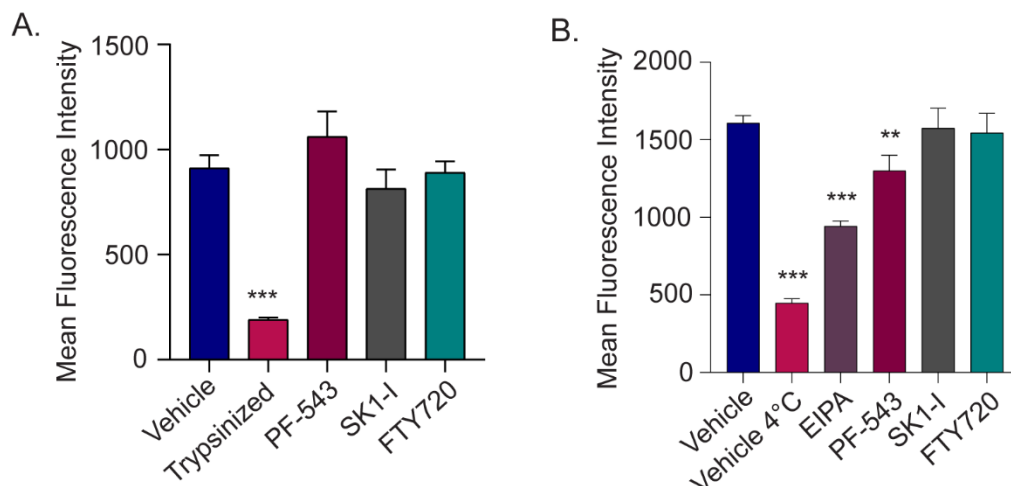
Figure 5. SK inhibitors do not interfere with attachment and have minimal or no effect on

internalization

HT1080 cells were pre-treated with vehicle (DMSO, 0.1%), PF-543 (10 µM), SK1-I (2.5 µM),

FTY720 (2.5 µM), or EIPA (30 µM) for 1 hour. In (A), cells were then detached and incubated

with GFP-VLPs harbouring EBOV GFP at 4 ℃. Cells were washed to remove unbound VLPs

and a subset of cells were trypsinized to remove bound VLPs as a negative control. Cells were

incubated with SYTOX red dead cell stain prior to analysis of fluorescence by flow cytometry.

(B) GFP-VLPs harbouring EBOV GP were pre-bound to treated cells by spinoculation at 4 ℃,

washed, and either incubated again with vehicle or inhibitor at 37 ℃, or vehicle alone at 4 ℃.

Cells were then trypsinized to remove bound VLPs, washed, and treated with SYTOX red dead

cell stain prior to analysis of fluorescence by flow cytometry. Results are expressed as mean ±

s.d. and are representative of three experiments. Variance was analyzed by one-way ANOVA,

followed by Dunnett's multiple comparisons test to determine significance. ** $p < 0.01$, *** $p <$

0.001.

257

258   *Entry of pre-cleaved EBOV VLPs is inhibited by sphingosine kinase inhibitors*

259   A critical post-internalization EBOV entry step is the cleavage of EBOV GP by

260   endosomal cathepsin proteases such as cathepsin B (1). Interestingly, a previous study suggested

261   that SK1-I treatment results in enlarged vacuoles that lack cathepsin B activity, therefore we also

262   assessed if the SK inhibitors may prevent GP-mediated cleavage by cathepsins (27). To

263   investigate this, we experimentally mimicked cathepsin cleavage by pre-cleaving EBOV VLPs

264   with thermolysin. We assessed entry of uncleaved and cleaved VLPs in HT1080 cells treated

265   with a cathepsin B inhibitor, Ca074, in addition to the SK inhibitors. As expected, Ca074 had

266   reduced potency on cleaved VLPs compared to the uncleaved VLPs (Figure 6). In contrast, the

267   SK inhibitors were equally potent at inhibiting entry of the cleaved and uncleaved VLPs,

268   suggesting that their primary mechanism of action is not to inhibit Cathepsin B-mediated

269   cleavage of EBOV GP.

270
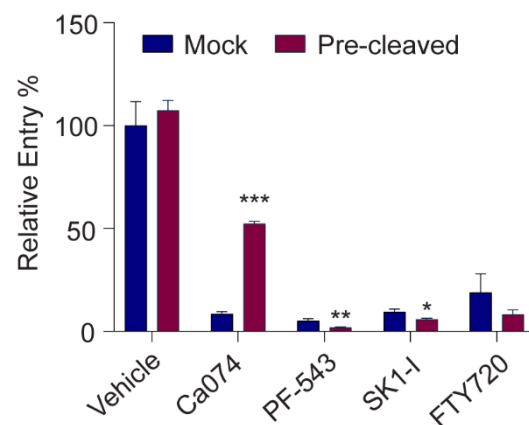
271   **Figure 6. Pre-cleaving EBOV GP does not rescue the SK inhibitor entry block**
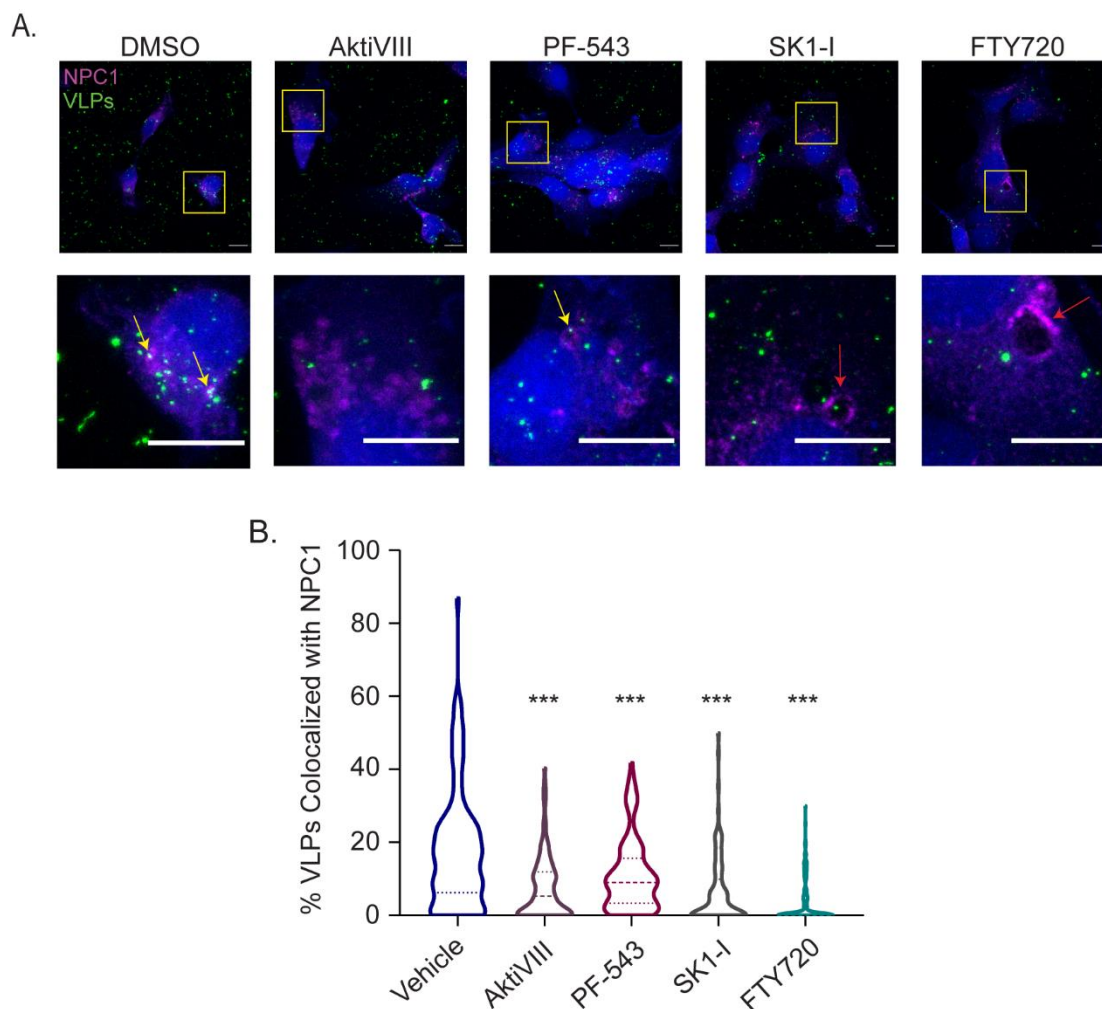
272   HT1080 cells were pre-treated with vehicle (DMSO, 0.1%), Ca074-Me (2.5 µM), PF-543 (10

273   µM), SK1-I (2.5 µM), or FTY720 (2.5 µM) for 1h prior to incubation with βlam VLPs

274   harbouring either thermolysin cleaved (pre-cleaved) or mock cleaved EBOV GP. Relative entry

275   % was determined by measuring the percentage of inhibitor-treated cells with cleaved βlam

276   substrate (CCF2) compared to vehicle-treated cells. Results are expressed as mean ± s.d. and are

277   representative of three experiments. Unpaired t-tests were performed to determine significance

278   between mock and pre-cleaved samples per inhibitor treatment. * $p < 0.05$, ** $p < 0.01$, *** $p <$

279   0.001.

280

281   ***Sphingosine kinase inhibitors interfere with trafficking of EBOV to NPC1+ intracellular***

282   ***compartments***

283   Since the SK inhibitors did not significantly prevent attachment and internalization, we

284   next sought to assess whether they blocked virus endolysosomal trafficking to the EBOV

285   receptor, NPC1. For these experiments, we utilized fluorescent VLPs harbouring EBOV GP^{F535R},

286   which can bind to NPC1 following cathepsin cleavage but cannot undergo fusion, therefore

287   allowing us to visualize accumulation of VLPs in NPC1+ compartments (5). As a control, we

288   used Akt Inhibitor VIII, which has been previously shown to result in accumulation of EBOV in

289   early endosomal compartments (17, 18). We determined the percentage of fluorescent VLPs

290   colocalizing with immunostained NPC1 in inhibitor treated cells compared to vehicle alone and

291   found a decrease in the percentage of VLPs per cell that colocalized with NPC1 for all three SK

292   inhibitors (Figure 7AB), suggesting that the SK inhibitors interfere with endosomal trafficking.

293   We also observed the presence of dilated intracellular vesicles in SK1-I and FTY720 treated cells

294   that were not present in vehicle or PF-543 treated cells (Figure 7A, red arrows). This is

295   consistent with recent studies demonstrating that treatment with sphingosine or sphingosine

296   analogs, including SK1-I and FTY720, induce rapid formation of enlarged intracellular vesicles

297   in cells (26, 27). Since such vesicles are often indicative of defects in endosomal trafficking,

298   their presence also supports a model by which treatment with the SK inhibitors result in

299   endosomal trafficking defects.

300

301   *Figure 7. SK inhibitors block trafficking of EBOV VLPs to NPC1*

302   (A) HT1080 cells were pre-treated with vehicle (DMSO, 0.1%), AktiVIII (10 µM), PF-543 (10

303   µM), SK1-I (2.5 µM), or FTY720 (2.5 µM) for 1h, followed by incubation with GFP-VLPs

304   (Green) harbouring the fusion deficient ΔM GPF535R for 3h. After 2.5h, CMAC cytoplasmic

305   dye (Blue) was added to the media for the remaining 30 minutes of the incubation. Cells were

306   then fixed, permeabilized, and immunostained with anti-NPC1 and DY-650 conjugated

307   antiserum (Magenta). Cells were imaged on a LSM800 confocal microscope (Zeiss). Displayed

308   images are maximum intensity Z-projections, yellow arrows indicate colocalization of VLPs and

309   NPC1, red arrows point to dilated intracellular vesicles, bar = 10 µm. (B) Colocalization between

310   VLPs and NPC1 was analyzed using Imaris software (Bitplane). Results are expressed as mean ±

311   s.d. and are of three experiments. Variance was analyzed by one-way ANOVA, followed by

312   Dunnett's multiple comparisons test to determine significance. *** p < 0.001.

313

The endolysosomal trafficking defect induced by the SK inhibitors is independent of S1P Receptor (S1PR) signaling

314   ***The endolysosomal trafficking defect induced by the SK inhibitors is independent of S1P***

315   ***Receptor (S1PR) signaling***

316   S1P, the product of SKs, is a bioactive sphingolipid involved in regulating cell growth,

317   survival, and migration (48). It is well-characterized for binding to cell surface S1PRs and

318   activating signaling cascades such as the PI3K-Akt pathway (23, 49, 50). Since Akt signaling

319   was shown to be important for EBOV trafficking and given that SK inhibitors were previously

320   shown to inhibit Akt phosphorylation, we hypothesized that the SK inhibitors block EBOV

321   trafficking by preventing S1P activation of S1PRs, therefore preventing subsequent Akt

322   activation (16-18, 51). To test this hypothesis and dissect the effect of SKs and S1PR signalling,

323   we evaluated the antiviral activity of FTY-720-Phosphate, which inhibits S1PR signaling by

324   inducing S1PR endocytosis and degradation but, unlike FTY-720, cannot enter the cell and

325   therefore does not inhibit SKs (43, 52, 53). Cells were pre-treated for one hour with FTY-720 or

326   FTY-720-Phosphate and entry of VLPs harbouring EBOV GP or VSV G was evaluated. We

327   found that FTY-720-Phosphate had no effect on EBOV-GP mediated entry while FTY-720

328   drastically blocked entry at the same concentration (Figure 8A), suggesting that the trafficking

329   defect caused by SK inhibitors is not a result of reduced signaling through S1PRs.

308   images are maximum intensity Z-projections, yellow arrows indicate colocalization of VLPs and

309   NPC1, red arrows point to dilated intracellular vesicles, bar = 10 µm. (B) Colocalization between

310   VLPs and NPC1 was analyzed using Imaris software (Bitplane). Results are expressed as mean ±

311   s.d. and are of three experiments. Variance was analyzed by one-way ANOVA, followed by

312   Dunnett's multiple comparisons test to determine significance. *** p < 0.001.

313

314   ***The endolysosomal trafficking defect induced by the SK inhibitors is independent of S1P***

315   ***Receptor (S1PR) signaling***

316   S1P, the product of SKs, is a bioactive sphingolipid involved in regulating cell growth,

317   survival, and migration (48). It is well-characterized for binding to cell surface S1PRs and

318   activating signaling cascades such as the PI3K-Akt pathway (23, 49, 50). Since Akt signaling

319   was shown to be important for EBOV trafficking and given that SK inhibitors were previously

320   shown to inhibit Akt phosphorylation, we hypothesized that the SK inhibitors block EBOV

321   trafficking by preventing S1P activation of S1PRs, therefore preventing subsequent Akt

322   activation (16-18, 51). To test this hypothesis and dissect the effect of SKs and S1PR signalling,

323   we evaluated the antiviral activity of FTY-720-Phosphate, which inhibits S1PR signaling by

324   inducing S1PR endocytosis and degradation but, unlike FTY-720, cannot enter the cell and

325   therefore does not inhibit SKs (43, 52, 53). Cells were pre-treated for one hour with FTY-720 or

326   FTY-720-Phosphate and entry of VLPs harbouring EBOV GP or VSV G was evaluated. We

327   found that FTY-720-Phosphate had no effect on EBOV-GP mediated entry while FTY-720

328   drastically blocked entry at the same concentration (Figure 8A), suggesting that the trafficking

329   defect caused by SK inhibitors is not a result of reduced signaling through S1PRs.

330   To further explore if FTY-720 and FTY-720-Phosphate reduce S1PR mediated PI3K-Akt

331   pathway activation, we treated cells with the inhibitors and assessed Akt phosphorylation by

332   immunoblot. As a positive control, we added S1P to vehicle-treated cells and found that S1P

333   treatment increased the levels of phosphorylated Akt in cells. Interestingly, while treatment with

334   FTY-720 did not alter phosphorylated Akt levels compared to vehicle treated cells, treatment

335   with FTY-720-Phosphate increased Akt phosphorylation to a similar extent as S1P treated cells

336   (Figure 8B). This suggests that FTY-720-Phosphate induces activation of S1PRs prior to

337   inducing their degradation, a result that is consistent with previous reports in the literature (53).

338   Therefore, the lack of entry inhibition seen after FTY-720-Phosphate treatment does not fully

339   rule out the possibility that the antiviral activity of the SK inhibitors is due to a reduction in S1P

340   signaling through cell surface S1PRs.

341   To address this, we performed an add-back experiment where S1P was added to inhibitor

342   treated cells prior to virus addition. If the entry and trafficking defects observed after SK

343   inhibitor treatment are due to a decrease in S1P signaling through S1PRs, adding extracellular

344   S1P should rescue the inhibitory entry effects mediated by the SK inhibitors. Importantly, we

345   found that S1P addition did not rescue EBOV entry in the presence of PF-543, SK1-I, or

346   FTY720 (Figure 8C). This result strongly suggests that the trafficking defect observed after

347   treatment with the SK inhibitors is not due to reduced S1P signaling through S1PRs. Further

348   work needs to be done to elucidate the precise molecular mechanism by which inhibiting SKs

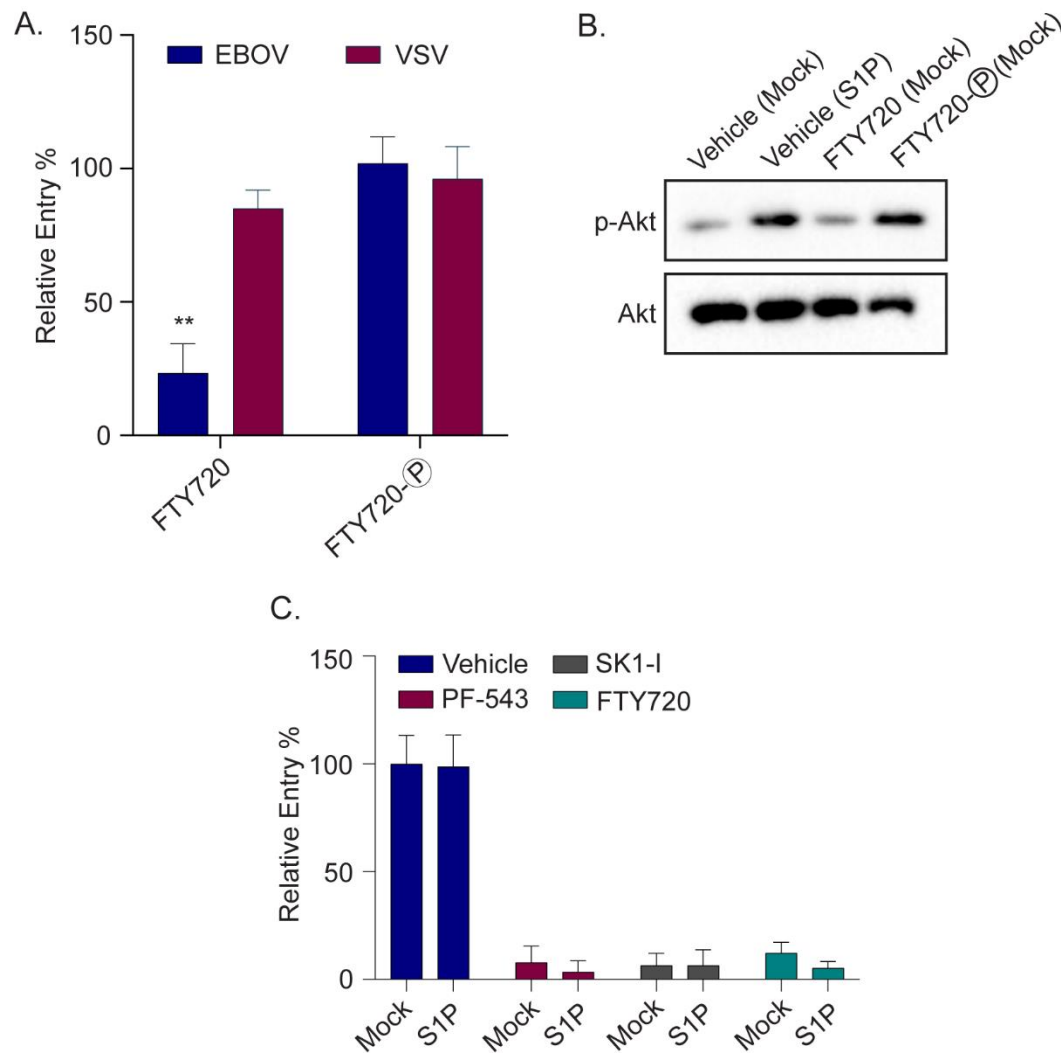349   results in an endosomal trafficking defect that blocks EBOV entry.

Figure 8. S1PR agonist does not reduce EBOV entry and S1PR activation by S1P does not rescue EBOV infection in inhibitor treated cells

(A-B) HT1080 cells were pre-treated with vehicle (DMSO, 0.1%), FTY720 (2.5 µM), or FTY720-Phosphate (2.5 µM) for 1h prior to (A) infection with βlam VLPs harbouring EBOV GP or VSV G, or (B) stimulation with S1P (125 nM) or mock. In (A), relative entry % was determined by measuring the percentage of inhibitor-treated cells with cleaved βlam substrate (CCF2) compared to vehicle-treated cells. In (B), cells were lysed and immunoblotted for phosphorylated Akt (p-Akt S473) or total Akt. (C) HT1080 cells were pre-treated with vehicle

359   (DMSO, 0.1%), PF-543 (10 µM), SK1-I (2.5 µM), or FTY720 (2.5 µM), stimulated with S1P

360   (125 nM) or mock, and infected with βlam VLPs harbouring EBOV GP. Relative entry % was

361   determined by measuring the percentage of inhibitor-treated cells with cleaved βlam substrate

362   (CCF2) compared to vehicle-treated cells. Results are expressed as mean ± s.d. of triplicates and

363   are representative of three experiments. Unpaired t-tests were performed to determine

364   significance between treatments. ** $p < 0.01$.

365

366   *Sphingosine kinase inhibitors reduce entry of other late penetrating viruses*

367   The host factors important for EBOV intracellular trafficking may be shared with other

368   viruses whose entry receptor or other triggering factors are also localized in late endosomes. As

369   such, it is plausible that entry mediated by the GP of these viruses may also be inhibited by the

370   SK inhibitors. Therefore, we tested the ability of the SK inhibitors to block entry of a panel of

371   enveloped viruses that require various extents of endosomal trafficking in all or some of the cell

372   types that they infect. Specifically, we tested Marburg virus (MARV), a related filovirus that

373   shares its entry receptor with EBOV, as well as Junin virus (JUNV), Influenza A virus (IAV),

374   and LFV, all of which require low pH for entry, while LFV further requires the lysosomal

375   protein LAMP-1 (2, 3, 28, 29, 31, 54-58). As controls, we included VSV, which undergoes

376   fusion in early endosomes, and Nipah virus (NiV), which requires its entry receptor, ephrinB2, to

377   mediate fusion at the cell surface (59-62). To explore the requirement of SKs for entry of these

378   viruses, we utilized MLV pseudotypes harbouring their respective viral fusion proteins and

379   tested entry in the presence of the SK inhibitors. While the SK inhibitors were the most potent at

380   inhibiting EBOV entry, they also significantly inhibited MARV entry, and to a lesser extent LFV

381   and JUNV (Figure 9A). Unexpectedly, these inhibitors either enhanced IAV entry, as was the

382   case for PF-543 and SK1-I, or had no effect, as was the case for FTY720 (Figure 9A). Lastly, we

383   found that PF-543 and SK1-I did not reduce VSV or NiV entry, and while FTY720 slightly

384   reduced VSV entry, it was not to the same extent as the other viruses (Figure 9A).

385   In addition to the aforementioned viruses, many coronaviruses also require triggering

386   factors in late endosomes to mediate entry in some cell types. Therefore, we utilized lentivirus

387   pseudotypes to examine entry mediated by the spike protein of the coronaviruses SARS-CoV-1

388   and middle eastern respiratory syndrome coronaviruses (MERS) in HT1080 cells. Importantly, in

389   these cells, SARS-CoV-1 S-mediated entry is dependent on cathepsin activity (Figure 9B),

390   indicating a requirement for late endosomal trafficking. Accordingly, we found that all SK

391   inhibitors drastically inhibited SARS-CoV-1 entry, while only PF-543 had a significant effect for

392   MERS entry (Figure 9C). Lastly, we tested whether the most potent inhibitor for inhibiting

393   SARS-CoV-1 entry, SK1-I, also inhibited infection of replication competent SARS-CoV-2. We

394   found that SK1-I inhibited infection of SARS-CoV-2 in Huh7.5 cells in a dose-dependent

395   manner (Fig. 9D). Taken together, these results suggest that sphingosine kinases are important

396   host factors that help facilitate viral entry of a range of enveloped viruses that enter cells through

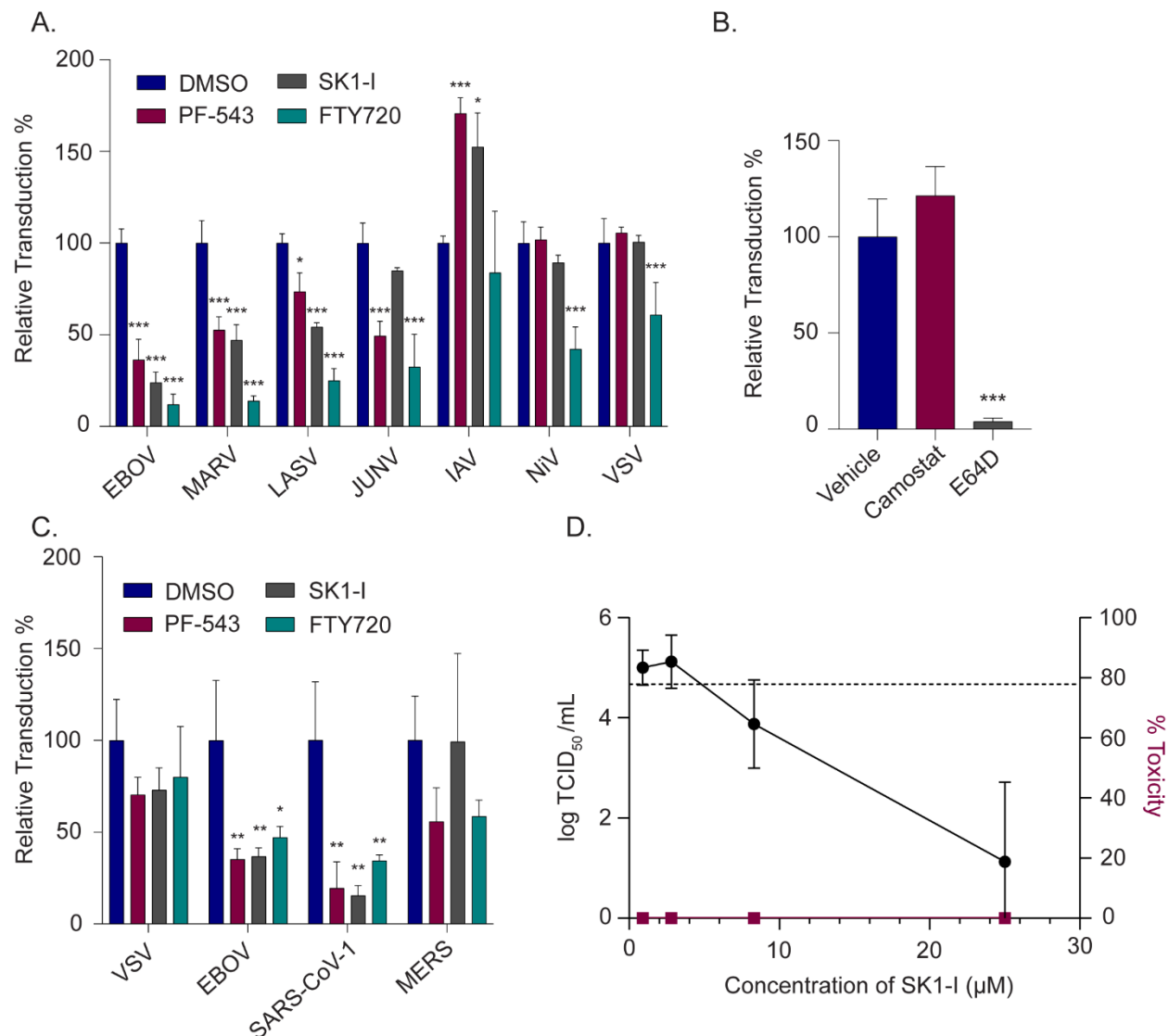397   endosomes and therefore could serve as host targets for novel pan-viral antiviral therapies.

398

Figure 9. Sphingosine kinase inhibitors inhibit entry of late penetrating viruses and SARS-

CoV-2 infection of Huh7.5 cells

(A-C) HT1080 cells treated with vehicle (DMSO, 0.1%), PF-543 (10 μM), SK1-I (2.5 μM),

FTY720 (2.5 μM), Camostat (25 μM), or E64D (10 μM) for 1h were transduced with (A) MLV

pseudotypes or (B,C) lentiviral pseudotypes, encoding lacZ and harbouring the fusion proteins of

the indicated viruses. Relative transduction % was determined by quantifying LacZ positive

inhibitor treated cells compared to vehicle treated cells. (D) Huh7.5 cells treated with vehicle or

406   increasing concentrations of SK1-I were infected with replication-competent SARS-CoV-2. 48

407   hpi, supernatant was collected and used directly to measure the TCID50. Results are expressed as

408   mean ± s.d. of triplicates and are representative of three experiments. Variance was analyzed by

409   one-way ANOVA, followed by Dunnett's multiple comparisons test to determine significance. *

410    $p < 0.05$, ** $p < 0.01$, *** $p < 0.001$.

411

Discussion

Entry of enveloped viruses into host cells requires fusion between the viral and host cell membranes, a process mediated by viral fusion proteins. For EBOV and other viruses, cellular proteins important for the priming and/or triggering of viral fusion proteins are localized in late-endosomes and lysosomes. Therefore, cellular entry of these viruses requires internalization and endolysosomal trafficking. In this study, we investigated SK inhibitors and characterized the role of SKs in EBOV entry. We found that SKs were required for EBOV trafficking to late intracellular vesicles containing the viral receptor and, accordingly, SK inhibitors also blocked infection by other viruses that use late endosomes/lysosomes for membrane fusion and entry. Our studies highlight an important role for SKs in endosomal trafficking and suggest that SK inhibitors have the potential to be developed for pan-antiviral therapy.

Signaling lipids play critical roles in endocytosis and endocytic trafficking (63, 64) and lipid modifying enzymes have been implicated to be important for EBOV entry; these include PIKfyve, diacylglycerol kinases (DGKs), and acid sphingomyelinases (ASMase) (13, 16, 65). For instance, EBOV was found to associate with lipid rafts rich in sphingomyelin (SM) and ASMases, and knockdown of ASMase inhibited EBOV entry (65). ASMase hydrolyses SM to ceramide, which can be converted to sphingosine and subsequently S1P via SKs. Ceramide has been implicated in lipid raft expansion and is more favorable compared to SM to promote membrane curvature and macropinocytosis (66). Interestingly, previous studies have demonstrated that SK1 associates with membranes of high curvature including macropinosomes and speculate that endocytosis may correlate with the conversion of SM to sphingosine, which can flip across the membrane and be converted to S1P by SKs (67). In our study, we also found that treatment with the SK1 inhibitor, PF-543, slightly reduced internalization of EBOV,

435   suggesting that SK1 may play a small role in macropinocytic uptake of EBOV (Figure 4B).

436   Interestingly, another study showed that a SK1 activator, K6PC-5, inhibited EBOV GP-mediated

437   entry (21). Therefore, taken with our current study, this suggests that interfering with S1P

438   production, whether it be positively or negatively, leads to inefficient EBOV entry. Although the

439   authors did not investigate the specific entry step that is inhibited in the presence of K6PC-5,

440   they found that the antiviral activity was independent of S1P receptors, which is also congruent

441   with our findings (21). The specific role(s) of S1P during entry and whether the lipid

442   composition of cellular membranes at the site of EBOV attachment or internalisation changes

443   remains to be investigated.

444   Here we show that all SK inhibitors prevented EBOV from trafficking to late-endosomes

445   and/or lysosomes containing NPC1 (Figure 4) suggesting that SKs play critical roles in

446   endosomal trafficking. Interestingly, a few other studies have also implicated SKs to be

447   important for proper endosomal maturation and fusion (26, 27). In a previous study, treatment

448   with the sphingosine analogues SK1-I and FTY720 resulted in the formation of dilated

449   intracellular vesicles that are positive for late endosomal markers Rab7a and LAMP-1,

450   suggesting that the trafficking block observed for EBOV after treatment with these inhibitors

451   occurs at the late endosome step (26, 27). Furthermore, Young et al. found that the vacuolization

452   is independent of S1P signaling, as pre-treatment with FTY720-Phosphate did not alter the SK1-

453   I/FTY720 induced vacuole formation (27). Moreover, they show that overloading endosomal

454   membranes with sphingosine results in similar vacuole formation and that treatment with PF-543

455   delays clearance (27). Our data indicates that while PF-543, a SK inhibitor that is not a

456   sphingosine analogue, does not induce formation of dilated vesicles, it does induce a similar

457   endocytic trafficking defect (Figure 4C and D). This not only provides an explanation for the

458   mechanism of antiviral activity of our SK inhibitors but also points to some potential areas for

459   future investigations of the role of sphingosine, SKs, and S1P in the regulation of endolysosomal

460   trafficking.

461   In addition to blocking EBOV entry, the SK inhibitors tested also inhibited entry of other

462   late penetrating viruses. For example, MARV, a related filovirus, was sensitive to the inhibitory

463   effects of the SK inhibitors, although not to the same extent as EBOV (Figure 5A). Similarly,

464   LFV entry was slightly blocked by the SK inhibitors, but was significantly less sensitive in

465   comparison to EBOV (Figure 5A). These differences may be attributed to the ability of both

466   MARV, and even more so, LFV, to undergo fusion in earlier endocytic compartments (4, 58).

467   Studies have shown that although MARV does require NPC1 for fusion, the MARV GP is

468   significantly less stable than EBOV GP and although proteolytic triggering of MARV GP is

469   required for entry, MARV is less dependent on cathepsins B and L (4, 68, 69). This suggests that

470   MARV GP-mediated fusion may be able to occur in earlier endocytic compartments compared to

471   EBOV. Similarly, a recent study suggested that LFV fusion may be able to occur in early

472   endosomes that contain only a small amount of the entry receptor LAMP-1 (58). We also tested

473   the effect of the SK inhibitors on coronavirus entry. For coronaviruses, the site of entry depends

474   on the expression of host proteases required to cleave the spike protein for activation (36). In our

475   study, we tested the effects of the SK inhibitors in cell types lacking surface proteases to allow

476   for entry via a route that requires endosomal trafficking. We found that the SK inhibitors

477   inhibited entry and/or infection by SARS-CoV-1, SARS-CoV-2, and to a lesser extent, MERS

478   (Figure 9). Together, our data strongly suggests that the SK inhibitors block a late trafficking

479   step, and that the efficacy of these inhibitors as antiviral agents will depend on the location of

480   fusion triggering among different viruses.

481   In this study, we identified sphingosine kinases as host factors required for viral entry of

482   EBOV and that of other late-penetrating viruses. We found that inhibition of SKs impairs

483   endosomal trafficking and that this occurs independently of S1P signaling through S1PRs at the

484   cell surface. Importantly, since entry of many enveloped viruses requires endosomal trafficking,

485   small molecule inhibitors of SKs may be promising candidates for the development of broad-

486   spectrum antiviral therapeutics that could prevent infection of both current and newly emerging

487   viruses.

488

489

Materials and Methods

490

Cell lines, antibodies, and inhibitors

491

492   HEK293T cells (ATCC) were cultured in Dulbecco's Modified Eagle Medium (DMEM,

493   Wisent), while HT1080 and Vero cells (ATCC) were cultured in Minimum Essential Medium

494   (MEM, Sigma). Both culture media were supplemented with 10% Fetal Bovine Serum (FBS,

495   Sigma), 0.3 mg/mL L-glutamine, 100 U/mL penicillin, and 100 µg/mL streptomycin (Wisent).

496   Cells were maintained at 37 °C in 5% CO_2 at 100% relative humidity.

497   Primary antibodies used were NPC1 (ab134113, Abcam), Akt (9272S, Cell Signaling

498   Technology), phospho-Akt S473 (92721S, Cell Signaling Technology), GAPDH (ab8245,

499   Abcam), SK1 (12071S, Cell Signaling Technology), SK2 (32346S, Cell Signaling Technology)

500   and pan-filovirus anti-GP antibody (21D10, IBT Bioservices). Secondary antibodies used were

501   goat anti-rabbit IgG HRP-linked (7074S, Cell Signaling Technology), anti-mouse IgG HRP-

502   linked (7076S, Cell Signaling Technology) and DY650 sheep anti-rabbit (ab96926, Abcam).

503   PF-543 (Cayman Chemical), SK1-I (BML-258, Enzo Life Sciences Inc.), FTY720

504   (Cayman Chemical), FTY720 Phosphate (Cayman Chemical), 5-(N-ethyl-N-isopropyl)-

505   Amiloride (EIPA, Cayman Chemical), and Akt Inhibitor VIII (Cayman Chemical) were prepared

506   in DMSO, aliquoted, and stored at -20 °C prior to use. PF-543 derivatives were synthesized as

507   described in supplementary information. Sphingosine-1-phosphate (d18:1, Cayman Chemical)

508   was prepared in a methanol:water (95:5), mixture was heated and sonicated for dissolution, and

509   stored in glass vials at -20 °C. Prior to use, the methanol:water solution was evaporated under a

510   N_2 stream and a 125 µM stock solution was prepared in 4 mg/mL fatty acid free Bovine Serum

511   Albumin (Sigma) in PBS and stored at -20 °C for up to 3 months.

Plasmids and DsiRNA

512

513   Plasmids encoding the virus glycoproteins EBOV Δmucin GP, EBOV Δmucin GP^{F535R},

514 MARV GP, VSV-G, LFV GP, NiV F and G fusion proteins, IAV Vict HA and 1918 NA, the

515 MLV packaging plasmid, and MLV retroviral vector encoding LacZ were kind gifts of Dr. James

516 Cunningham (Brigham and Women's Hospital, Boston, Massachusetts). Plasmids encoding the

517 EBOV NP and EBOV VP40-β-lactamase or GFP were kind gifts of Dr. Lijun Rong, University

518 of Illinois. The plasmids encoding human ACE2 and SARS-CoV-S were a kind gifts of Dr.

519 Hyeryun Choe (The Scripps Research Institute, Jupiter, Florida). Plasmid encoding the MERS-

520 CoV-S was a kind gift of Thomas Gallagher (Loyola University Chicago, Chicago, Illinois). LV-

521 Lac was a gift from Inder Verma (Addgene plasmid # 12108, (70)) and psPAX2 was a gift from

522 Didier Trono (Addgene plasmid # 12260).

523   Predesigned DsiRNAs for SK1 (hs.Ri.SPHK1.13.1; duplex sequences:

524 5'-rGrCrGrUrCrArUrGrCrArUrCrUrGrGrUrUrCrUrArCrGrUrGCG -3';

525 3'- rCrGrCrArCrGrUrArGrArArCrArGrArUrGrCrArUrGrArCrGrCrCrA-5'), SK2

526 (hs.Ri.SPHK213.1; duplex sequences:

527 5'-rCrCrCrUrGrArArArArCrUrArArArArCrArArGrCrUrUrGrGrUAC-3',

528 3'-rGrUrArCrCrArArGrCrUrUrGrUrUrUrUrArGrUrUrUrCrArGrGrGrCrU-5'), and negative

529 control dsiRNA (51-01-14-04) were purchased from Integrated DNA Technologies, Inc.

530 (Coralville, Iowa).

Viral pseudotype and viral-like particle production

531

532   Murine leukemia virus and lentivirus pseudotypes were prepared by co-transfecting

533 HEK293T cells with the packaging plasmid gag-pol or psPAX2, MLV retroviral or lentiviral

534 vector encoding LacZ, and a plasmid encoding the glycoprotein of interest (EBOV Δmucin GP,

535   MARV GP, LFV GP, NiV F and G (1:1), Junin GPC, IAV envelope proteins (Vict HA, 1918

536   NA), SARS-CoV-1 Spike, MERS Spike, or VSV-G) at a 1:1:1.25 ratio respectively. Similarly,

537   EBOV viral-like particles (VLPs) were prepared by co-transfecting HEK293T cells with

538   plasmids encoding the EBOV nucleoprotein (NP), EBOV VP40 fused to β-lactamase (βlam) or

539   GFP, and the viral glycoprotein of interest (EBOV Δmucin GP, EBOV Δmucin GP^{F535R}, or VSV

540   G) at a 1:1:1.25 ratio. Transfections were performed using the jetPRIME transfection reagent

541   (Polyplus transfection) according to the manufacturers protocol. Cell supernatants were

542   harvested at 48, 72, and 96 h post-transfection. MLVs and lentiviruses supernatants were passed

543   through a 0.45µm filter and VLPs supernatants pre-cleared by centrifugation at 4,000g for 5min.

544   Pseudotypes and VLPs were then concentrated by ultracentrifugation (20,000 RPM, 4 ⁰C, 1.5h,

545   Beckman Coulter Optima XPN-100, SW32Ti rotor) through a 20% (*w/v*) sucrose cushion. Pellets

546   were re-suspended in PBS, aliquoted, and stored at -80 ⁰C.

547   ***Virus entry assays***

548   For MLV and lentivirus pseudotype transduction assays, HT1080 cells were seeded and

549   grown to approximately 60% confluency in white 96-well pates. Cells were pre-incubated with

550   inhibitor or vehicle (DMSO) in serum-free MEM containing 5 µg/mL polybrene. MLV or

551   lentivirus pseudotypes encoding LacZ and harbouring the viral fusion protein of interest were

552   added to the media. 4-6 hours after virus addition, the media was replaced with MEM containing

553   15 mM NH$_4$Cl and supplemented with 10% FBS (Sigma), 0.3 mg/mL L-glutamine, 100 U/mL

554   penicillin, and 100µg/mL streptomycin (Wisent). Approximately 12 hours later, the media was

555   replaced with complete MEM (without NH$_4$Cl) and cells incubated an additional 48 hours.

556   Transduced (LacZ+) cells were quantified using the Beta-Glo Assay System (Promega, Madison,

557 Wisconsin) following the manufacturers' protocol. Luminescence was measured using a Synergy

558 Neo2 multi-mode plate reader (BioTek Instruments, Winooski, Vermont).

559 For the VLP entry assays, HT1080 cells were seeded and grown to 90% confluency. For

560 experiments with inhibitors, cells were pre-treated with the inhibitors or vehicle (DMSO) for 1

561 hour in serum-free MEM. For S1P experiments, cells were pre-treated for 1 hour in serum-free

562 MEM with inhibitor or vehicle, and S1P (125 nM) was added 10 minutes prior to virus addition.

563 VP40-βlam VLPs harbouring EBOVΔM or VSV-G were added at a MOI between 0.2 and 0.4. 3

564 hours post infection, cells were loaded with a β-lactamase cleavable FRET substrate, CCF2-AM

565 (ThermoFisher Scientific, Waltham, Massachusetts), according to manufacturer's protocol and

566 supplemented with 15 mM NH_4Cl and 250 μM probenecid (Sigma). Cells were then incubated

567 for 1h at room temperature in the dark, washed with PBS, trypsinized, and resuspended with 2%

568 FBS in PBS prior to analysis by flow cytometry (FACSCelesta or LSRFortessa, BD

569 Biosciences). Flow cytometry analysis was performed using the FlowJo software (BD

570 Biosciences) and infection was quantified by using uninfected controls to assess the percentage

571 of cells that underwent a shift from 530 nm to 460 nm emission, representing cleaved CCF2.

572 ***Sphingosine kinase 1/2 activity assay***

573 SK1 and SK2 specific master mixes were pre-equilibrated at room temperature and

574 prepared immediately before use. SK1 reaction buffer contained 100nM SK1 (R&D systems,

575 Minneapolis, Minnesota), 25uM NBD-Sph (Cayman Chemical Company, Ann Arbor,

576 Michigan), 30 mM Tris-HCl, pH 7.4, 0.05% Triton X-100, 150 mM NaCl, 10% glycerol, 1 mM

577 Na3VO4, 10 mM NaF, and 10 mM b-glycero-phosphate and SK2 reaction buffer contained

578 15nM SK2 (R&D systems, Minneapolis, Minnesota), 75 NBD-Sph, 30 mM Tris-HCl, pH 7.4,

579 0.05% Triton X-100, 200 mM KCl, and 10% glycerol. Solutions were vortexed and 18 ul of the

580   master mix was added per well of a 384-well black plates (ThermoFisher Scientific, Waltham,

581   Massachusetts), followed by the addition of 1ul of inhibitors at 20uM, for a final concentration

582   of 1uM. The assay was initiated with 1ul of 20× ATP-Mg (20 mM ATP, 200 mM MgCl2, 900

583   mM Tris-HCl, pH 7.4), after which the 384-well plate was shaken at 800 rpm for 1 min to allow

584   for complete mixing. After an incubation of 10 min (SK2) and 30 min (SK1) at room

585   temperature, fluorescence emission was measured with a Synergy Neo2 multi-mode plate reader

586   (BioTek Instruments, Winooski, Vermont) where the excitation wavelength was set at 550 nm,

587   and emission wavelength at 584 nm.

Pre-cleaved virus

589   βlam VLPs harboring EBOV Δmucin GP were incubated in 0.2 mg/mL thermolysin

590   (MilliporeSigma, Burlington, Massachusetts) or PBS (mock) for 30 minutes at 37ºC.

591   Phosphoramidon (MilliporeSigma,Burlington, Massachusetts) was then added to a final

592   concentration of 500 µM and the mixture was incubated on ice for 10 minutes. Pre-cleaved

593   (thermolysin-treated) and mock-cleaved (PBS-treated) samples were aliquoted and stored at -80

594   ºC.

DsiRNAs transfection and infection assays

596   HT1080 were cells grown to 90% confluency and transfected with the DsiRNAs using

597   Lipofectamine RNAiMAX (ThermoFisher Scientific, Waltham, Massachusetts) according to the

598   manufacturer's protocol. 24 hours post-transfection, cells were re-seeded for VLP entry assays,

599   which were conducted 48 hours post-transfection as described above, with the exception that

600   cells were pre-incubated in serum-free MEM that did not contain any inhibitor or vehicle. In

601   addition, 48 hours post-transfection, cells seeded for lysate preparation were washed once with

602   PBS, followed by the addition of lysis buffer (1% Triton X-100, 0.1% IGEPAL CA-630, 150mM

603   NaCl, 50mM Tris-HCl, pH 7.5) containing protease inhibitors (Cell Signaling Technology,

604   Danvers, Massachusetts). Proteins were resolved on SDS-polyacrylamide gels and transferred to

605   polyvinylidenedifluoride (PVDF) membranes. Membranes were blocked for 1h at room

606   temperature with blocking buffer (5% skim milk powder dissolved in 25mM Tris, pH 7.5,

607   150mM NaCl, and 0.1% Tween-20 [TBST]). PVDF membranes were then incubated overnight

608   at 4 °C with the appropriate primary antibody. The following day, blots were washed in TBST

609   and incubated with HRP-conjugated secondary antibody for 1h at room temperature. PVDF

610   membranes were then washed again, incubated in chemiluminescence substrate, and imaged

611   using the ChemiDoc XRS+ imaging system (Bio-Rad Laboratories, Hercules, California).

612   ***Replicative EBOV and SARS-CoV-2 Infection assays***

613   For infection assays with replication-competent EBOV, Vero cells were seeded onto

614   black 96 well plates with glass bottom wells. After 48 hours, cells were pre-treated for 1 hour

615   with vehicle (DMSO) or PF-543 in DMEM supplemented with 1% FBS. Ebola virus (Mayinga)

616   expressing GFP was added to media containing inhibitors or vehicle and incubated together for

617   15 minutes prior to addition of the mixture to the cells at a final MOI of 1. Control wells

618   containing no virus were also included. After infection, GFP expression was monitored daily

619   using a BioTek Synergy/HTX plate reader (BioTek Instruments, Winooski, Vermont). These

620   experiments were performed at the CL-4 facility at the National Microbiology Laboratory of the

621   Public Health Agency of Canada.

622   For infection assays with replication-competent SARS-CoV-2 (hCoV-19/Canada/ON-

623   VIDO-01/2020, GISAID accession# EPI_ISL_425177), Huh7.5 cells were seeded and once

624   adhered, inhibitor or vehicle was incubated with the cells at 2x concentration for 1 hour (71).

625   SARS-CoV-2 was then added to each well at an MOI of 0.01 and to give a final inhibitor

626   concentration of 1x. The inoculum + drug mixture was incubated on cells for 2-3 hours at 37 °C,

627   cells were then washed with MEM and media containing inhibitor or vehicle was added back to

628   cells and incubated for an additional 48h at 37 °C. Supernatant was then collected and used

629   directly to measure the TCID50/mL on Vero cells. These experiments were performed at the CL-

630   4 facility at the National Microbiology Laboratory of the Public Health Agency of Canada.

631   ***S1PR downstream signaling assay***

632   HT1080 cells were seeded and grown to 50% confluency, washed with PBS, and pre-

633   treated for 1 hour with inhibitor or vehicle (DMSO) in serum-free MEM. Cells were then

634   stimulated for 30 minutes with S1P prepared in 4 mg/mL fatty acid free Bovine Serum Albumin

635   (BSA) (MilliporeSigma) in PBS or mock-treated for 30 minutes with 4 mg/mL fatty acid free

636   BSA in PBS. Cells were then washed once with cold PBS and lysed in cold lysis buffer (1%

637   Triton X-100, 0.1% IGEPAL CA-630, 150mM NaCl, 50mM Tris-HCl, pH 7.5) containing

638   protease and phosphatase inhibitors (Cell Signaling). Proteins were resolved on SDS-

639   polyacrylamide gels (Bio-Rad) and transferred to polyvinylidenedifluoride (PVDF) membranes.

640   Membranes were blocked at RT with blocking buffer (5% skim milk powder in TBST containing

641   sodium orthovanadate (Na_3VO_4, 1mM, Alfa Aesar) and sodium fluoride (NaF, 10mM, VWR)).

642   After 1 hour of blocking, membranes were incubated overnight at 4°C with either the pAkt

643   antibody in 5% BSA in TBST containing Na_3VO_4 and NaF, or Akt antibody in 5% skim milk

644   powder in TBST. The following day, blots were washed in TBST and incubated with HRP-

645   conjugated secondary antibody for 1h at room temperature. After 3 more washes in TBST, the

646   membranes were incubated in chemiluminescence substrate and imaged using the ChemiDoc

647   XRS+ imaging system (Bio-Rad Laboratories).

648 *Attachment and internalization assays*

649   For the attachment assay, HT1080 cells were seeded and grown to 90% confluency. Cells

650 were pre-treated with serum-free MEM containing inhibitor or vehicle for 1 hour at 37 °C. The

651 cells were detached with 5 mM EDTA and resuspended in 2% FBS in PBS containing inhibitor

652 or vehicle. After incubation at 4 °C for 15 minutes, VP40-GFP EBOVΔM VLPs were added on

653 ice and incubated for 1 h at 4 °C to allow the virus to attach to the cell surface. As a control, one

654 set of vehicle treated cells was incubated with trypsin to remove bound virions. The cell and

655 virus mixtures were spun down and washed three times with cold PBS prior to resuspension in

656 2% FBS in PBS containing SYTOX Red dead cell stain (ThermoFisher) and analysis by flow

657 cytometry.

658   For the internalization experiments, HT1080 cells were seeded and grown to 90%

659 confluency. Cells were pre-treated with serum-free MEM containing inhibitor or vehicle

660 (DMSO) for 1 hour at 37°C. The cells were then incubated at 4°C for 15 minutes prior to

661 spinoculation of VP40-GFP EBOVΔM VLPs at 300 x g for 30 minutes. Cells were then washed

662 3x with cold PBS to removed unbound virions, pre-warmed media containing inhibitor or vehicle

663 was added, and cells were moved to 37 °C for 1 hour to allow for internalization. Cells were then

664 washed again with cold PBS and incubated with 0.5% trypsin-EDTA (Gibco) at 4 °C for 30

665 minutes to remove VLPs that were still at the surface. Cells were then distributed into tubes

666 containing cold PBS, spun down and washed twice with cold PBS, and finally resuspended in

667 2% FBS in PBS containing SYTOX Red dead cell stain (ThermoFisher) prior to analysis by flow

668 cytometry.

669   *Fluorescence microscopy and image analysis*

670   HT1080 cells were seeded onto coverslips that were coated with Poly-D-lysine (Sigma)

671   and grown to approximately 50% confluency. Cells were then pre-treated with inhibitors or

672   vehicle (DMSO) in serum-free MEM for 1 h followed by addition of VP40-GFP VLPs harboring

673   the fusion deficient EBOV Δmucin GP^{F535R}. Cells were incubated for 2.5 hours at 37 °C,

674   CellTracker Blue CMAC dye (ThermoFisher) was added according to manufacturer's protocol,

675   and cells were incubated for an additional 30 minutes. Cells were then washed with PBS, fixed

676   with formalin, permeabilized with 0.5% triton X-100, and blocked with 20% FBS in PBS for 30

677   minutes. Cells were then incubated with a NPC1 primary antibody (1:70) followed by a DY650

678   secondary antibody (1:400) and mounted with PermaFluor Aqueous Mounting medium

679   (ThermoFisher). Imaging was performed with a LSM800 confocal microscope (AxioObserver

680   Z1, Zeiss) using a 63x / 1.4NA oil Plan Apochromat objective. Approximately fifteen z-stacks

681   were acquired per image with a pixel size of 0.1 µm.

682   Image analysis was performed using Imaris software v. 8.4.2 (Bitplane). In brief, each

683   cell was modeled based on the CMAC cytoplasmic stain using the surfaces module, and VLPs

684   were modeled as spots. The number of spots per cell was then determined and the modeled spots

685   were assigned colocalization values based on intensity correlation to NPC1. Intensity thresholds

686   were manually set for each experiment but kept constant between experimental conditions. By

687   dividing the number of spots above the colocalization threshold by the total number of spots per

688   cell, the percentage of VLPs colocalizing with NPC1 was determined.

Acknowledgments

References

1. Chandran K, Sullivan NJ, Felbor U, Whelan SP, & Cunningham JM (2005) Endosomal Proteolysis of the Ebola Virus Glycoprotein Is Necessary for Infection. *Science* 308(5728):1643.

2. Cote M, *et al.* (2011) Small molecule inhibitors reveal Niemann-Pick C1 is essential for Ebola virus infection. *Nature* 477(7364):344-348.

3. Carette JE, *et al.* (2011) Ebola virus entry requires the cholesterol transporter Niemann-Pick C1. *Nature* 477(7364):340-343.

4. Misasi J, *et al.* (2012) Filoviruses require endosomal cysteine proteases for entry but exhibit distinct protease preferences. *J Virol* 86(6):3284-3292.

5. Brecher M, *et al.* (2012) Cathepsin cleavage potentiates the Ebola virus glycoprotein to undergo a subsequent fusion-relevant conformational change. *J Virol* 86(1):364-372.

6. Alvarez CP, *et al.* (2002) C-type lectins DC-SIGN and L-SIGN mediate cellular entry by Ebola virus in cis and in trans. *J Virol* 76(13):6841-6844.

7. Kondratowicz AS, *et al.* (2011) T-cell immunoglobulin and mucin domain 1 (TIM-1) is a receptor for Zaire Ebolavirus and Lake Victoria Marburgvirus. *Proceedings of the National Academy of Sciences* 108(20):8426-8431.

8. Hunt CL, Kolokoltsov AA, Davey RA, & Maury W (2011) The Tyro3 receptor kinase Axl enhances macropinocytosis of Zaire ebolavirus. *J Virol* 85(1):334-347.

9. Nanbo A, *et al.* (2010) Ebolavirus is internalized into host cells via macropinocytosis in a viral glycoprotein-dependent manner. *PLoS Pathog* 6(9):e1001121.

10. Saeed MF, Kolokoltsov AA, Albrecht T, & Davey RA (2010) Cellular entry of ebola virus involves uptake by a macropinocytosis-like mechanism and subsequent trafficking through early and late endosomes. *PLoS Pathog* 6(9):e1001110.

11. Mulherkar N, Raaben M, de la Torre JC, Whelan SP, & Chandran K (2011) The Ebola virus glycoprotein mediates entry via a non-classical dynamin-dependent macropinocytic pathway. *Virology* 419(2):72-83.

12. Shtanko O, Reyes AN, Jackson WT, & Davey RA (2018) Autophagy-Associated Proteins Control Ebola Virus Internalization Into Host Cells. *J Infect Dis* 218(suppl_5):S346-S354.

13. Stewart CM, *et al.* (2019) A Diacylglycerol Kinase Inhibitor, R-59-022, Blocks Filovirus Internalization in Host Cells. *Viruses* 11(3):206.

14. Simmons JA, *et al.* (2016) Ebolavirus Glycoprotein Directs Fusion through NPC1+ Endolysosomes. *J Virol* 90(1):605-610.

15. Bo Y, Qiu S, Mulloy RP, & Cote M (2020) Filoviruses Use the HOPS Complex and UVRAG To Traffic to Niemann-Pick C1 Compartments during Viral Entry. *J Virol* 94(16): e01002-01020.

16. Qiu S, *et al.* (2018) Ebola virus requires phosphatidylinositol (3,5) bisphosphate production for efficient viral entry. *Virology* 513:17-28.

17. Saeed MF, Kolokoltsov AA, Freiberg AN, Holbrook MR, & Davey RA (2008) Phosphoinositide-3 kinase-Akt pathway controls cellular entry of Ebola virus. *PLoS Pathog* 4(8):e1000141.

18. Stewart CM, *et al.* (2021) Ebola virus triggers receptor tyrosine kinase-dependent signaling to promote the delivery of viral particles to entry-conducive intracellular compartments. *PLoS Pathog* 17(1):e1009275.

752 19. Kuroda M, Halfmann P, & Kawaoka Y (2020) HER2-mediated enhancement of Ebola
753   virus entry. *PLOS Pathogens* 16(10):e1008900.
754 20. Kondratowicz AS, Hunt CL, Davey RA, Cherry S, & Maury WJ (2013) AMP-activated
755   protein kinase is required for the macropinocytic internalization of ebolavirus. *J Virol*
756   87(2):746-755.
757 21. Imre G, *et al.* (2021) The sphingosine kinase 1 activator, K6PC-5, attenuates Ebola virus
758   infection. *iScience* 24(4):102266.
759 22. Pitson SM (2011) Regulation of sphingosine kinase and sphingolipid signaling. *Trends*
760   *Biochem Sci* 36(2):97-107.
761 23. Bryan AM & Del Poeta M (2018) Sphingosine-1-phosphate receptors and innate
762   immunity. *Cell Microbiol* 20(5):e12836.
763 24. Maceyka M, Alvarez SE, Milstien S, & Spiegel S (2008) Filamin A links sphingosine
764   kinase 1 and sphingosine-1-phosphate receptor 1 at lamellipodia to orchestrate cell
765   migration. *Mol Cell Biol* 28(18):5687-5697.
766 25. Dharmawardhane S, *et al.* (2000) Regulation of macropinocytosis by p21-activated
767   kinase-1. *Mol Biol Cell* 11(10):3341-3352.
768 26. Lima S, Milstien S, & Spiegel S (2017) Sphingosine and Sphingosine Kinase 1
769   Involvement in Endocytic Membrane Trafficking. *J Biol Chem* 292(8):3074-3088.
770 27. Young MM, *et al.* (2016) Sphingosine Kinase 1 Cooperates with Autophagy to Maintain
771   Endocytic Membrane Trafficking. *Cell Rep* 17(6):1532-1545.
772 28. Jae LT, *et al.* (2014) Virus entry. Lassa virus entry requires a trigger-induced receptor
773   switch. *Science* 344(6191):1506-1510.
774 29. Li S, *et al.* (2016) Acidic pH-Induced Conformations and LAMP1 Binding of the Lassa
775   Virus Glycoprotein Spike. *PLOS Pathogens* 12(2):e1005418.
776 30. Cohen-Dvashi H, Cohen N, Israeli H, Diskin R, & Ross SR (2015) Molecular
777   Mechanism for LAMP1 Recognition by Lassa Virus. *Journal of Virology* 89(15):7584-
778   7592.
779 31. Cohen-Dvashi H, *et al.* (2016) Role of LAMP1 Binding and pH Sensing by the Spike
780   Complex of Lassa Virus. *Journal of Virology* 90(22):10329-10338.
781 32. Jae LT & Brummelkamp TR (2015) Emerging intracellular receptors for hemorrhagic
782   fever viruses. *Trends Microbiol* 23(7):392-400.
783 33. Matsuyama S, *et al.* (2010) Efficient Activation of the Severe Acute Respiratory
784   Syndrome Coronavirus Spike Protein by the Transmembrane Protease TMPRSS2.
785   *Journal of Virology* 84(24):12658-12664.
786 34. Glowacka I, *et al.* (2011) Evidence that TMPRSS2 Activates the Severe Acute
787   Respiratory Syndrome Coronavirus Spike Protein for Membrane Fusion and Reduces
788   Viral Control by the Humoral Immune Response. *Journal of Virology* 85(9):4122-4134.
789 35. Hoffmann M, *et al.* (2020) SARS-CoV-2 Cell Entry Depends on ACE2 and TMPRSS2
790   and Is Blocked by a Clinically Proven Protease Inhibitor. *Cell* 181(2):271-280.e278.
791 36. Koch J, *et al.* (2021) TMPRSS2 expression dictates the entry route used by SARS-CoV-2
792   to infect host cells. *The EMBO Journal* 40(16):e107821.
793 37. Benlarbi M, *et al.* (2022) Identification of a SARS-CoV-2 host metalloproteinase-
794   dependent entry pathway differentially used by SARS-CoV-2 and variants of concern
795   Alpha, Delta, and Omicron. *bioRxiv*.

796   38.   Simmons G, *et al.* (2005) Inhibitors of cathepsin L prevent severe acute respiratory
797   syndrome coronavirus entry. *Proceedings of the National Academy of Sciences of the*
798   *United States of America* 102(33):11876-11881.
799   39.   Ou X, *et al.* (2020) Characterization of spike glycoprotein of SARS-CoV-2 on virus entry
800   and its immune cross-reactivity with SARS-CoV. *Nature Communications* 11(1):1620.
801   40.   Shang J, *et al.* (2020) Cell entry mechanisms of SARS-CoV-2. *Proceedings of the*
802   *National Academy of Sciences* 117(21):11727-11734.
803   41.   Lozach PY, Huotari J, & Helenius A (2011) Late-penetrating viruses. *Current opinion in*
804   *virology* 1(1):35-43.
805   42.   Schnute ME, *et al.* (2012) Modulation of cellular S1P levels with a novel, potent and
806   specific inhibitor of sphingosine kinase-1. *Biochem J* 444(1):79-88.
807   43.   Paugh SW, Payne SG, Barbour SE, Milstien S, & Spiegel S (2003) The
808   immunosuppressant FTY720 is phosphorylated by sphingosine kinase type 2. *FEBS Lett*
809   554(1-2):189-193.
810   44.   Paugh SW, *et al.* (2008) A selective sphingosine kinase 1 inhibitor integrates multiple
811   molecular therapeutic targets in human leukemia. *Blood* 112(4):1382-1391.
812   45.   Simmons G, *et al.* (2003) Folate receptor alpha and caveolae are not required for Ebola
813   virus glycoprotein-mediated viral infection. *J Virol* 77(24):13433-13438.
814   46.   Schnute ME, *et al.* (2017) Discovery of a Potent and Selective Sphingosine Kinase 1
815   Inhibitor through the Molecular Combination of Chemotype-Distinct Screening Hits. *J*
816   *Med Chem* 60(6):2562-2572.
817   47.   Koivusalo M, *et al.* (2010) Amiloride inhibits macropinocytosis by lowering
818   submembranous pH and preventing Rac1 and Cdc42 signaling. *J Cell Biol* 188(4):547-
819   563.
820   48.   Rosen H, Stevens RC, Hanson M, Roberts E, & Oldstone MB (2013) Sphingosine-1-
821   phosphate and its receptors: structure, signaling, and influence. *Annual review of*
822   *biochemistry* 82:637-662.
823   49.   Bonnaud S, *et al.* (2010) Sphingosine-1-phosphate activates the AKT pathway to protect
824   small intestines from radiation-induced endothelial apoptosis. *Cancer Res* 70(23):9905-
825   9915.
826   50.   Wang H, Huang H, & Ding S-F (2018) Sphingosine-1-phosphate promotes the
827   proliferation and attenuates apoptosis of Endothelial progenitor cells via
828   S1PR1/S1PR3/PI3K/Akt pathway. *Cell Biology International* 42(11):1492-1502.
829   51.   Kapitonov D, *et al.* (2009) Targeting Sphingosine Kinase 1 Inhibits Akt Signaling,
830   Induces Apoptosis, and Suppresses Growth of Human Glioblastoma Cells and
831   Xenografts. *Cancer Research* 69:6915-6923.
832   52.   Brinkmann V, *et al.* (2002) The immune modulator FTY720 targets sphingosine 1-
833   phosphate receptors. *J Biol Chem* 277(24):21453-21457.
834   53.   Oo ML, *et al.* (2007) Immunosuppressive and anti-angiogenic sphingosine 1-phosphate
835   receptor-1 agonists induce ubiquitinylation and proteasomal degradation of the receptor.
836   *J Biol Chem* 282(12):9082-9089.
837   54.   Martinez MG, Cordo SM, & Candurra NA (2007) Characterization of Junín arenavirus
838   cell entry. *Journal of General Virology* 88(6):1776-1784.
839   55.   York J & Nunberg JH (2009) Intersubunit Interactions Modulate pH-Induced Activation
840   of Membrane Fusion by the Junín Virus Envelope Glycoprotein GPC. *Journal of*
841   *Virology* 83(9):4121-4126.

842 56. Stegmann T, Booy FP, & Wilschut J (1987) Effects of low pH on influenza virus.
843   Activation and inactivation of the membrane fusion capacity of the hemagglutinin.
844   *Journal of Biological Chemistry* 262(36):17744-17749.
845 57. Sieczkarski SB & Whittaker GR (2003) Differential requirements of Rab5 and Rab7 for
846   endocytosis of influenza and other enveloped viruses. *Traffic* 4(5):333-343.
847 58. Hulseberg CE, Fénéant L, Szymańska KM, & White JM (2018) Lamp1 Increases the
848   Efficiency of Lassa Virus Infection by Promoting Fusion in Less Acidic Endosomal
849   Compartments. *mBio* 9(1):e01818-01817.
850 59. Cureton DK, Massol RH, Saffarian S, Kirchhausen TL, & Whelan SP (2009) Vesicular
851   stomatitis virus enters cells through vesicles incompletely coated with clathrin that
852   depend upon actin for internalization. *PLoS Pathog* 5(4):e1000394.
853 60. Johannsdottir HK, Mancini R, Kartenbeck J, Amato L, & Helenius A (2009) Host cell
854   factors and functions involved in vesicular stomatitis virus entry. *J Virol* 83(1):440-453.
855 61. Bonaparte MI*, et al.* (2005) Ephrin-B2 ligand is a functional receptor for Hendra virus
856   and Nipah virus. *Proc Natl Acad Sci U S A* 102(30):10652-10657.
857 62. Negrete OA*, et al.* (2005) EphrinB2 is the entry receptor for Nipah virus, an emergent
858   deadly paramyxovirus. *Nature* 436(7049):401-405.
859 63. Li X, Garrity AG, & Xu H (2013) Regulation of membrane trafficking by signalling on
860   endosomal and lysosomal membranes. *The Journal of physiology* 591(18):4389-4401.
861 64. Qiu S & Côté M (2018) From hitchhiker to hijacker: pathogen exploitation of endosomal
862   phosphoinositides. *Biochemistry and Cell Biology* 97(1):1-9.
863 65. Miller ME, Adhikary S, Kolokoltsov AA, & Davey RA (2012) Ebolavirus requires acid
864   sphingomyelinase activity and plasma membrane sphingomyelin for infection. *J Virol*
865   86(14):7473-7483.
866 66. Gulbins E & Li PL (2006) Physiological and pathophysiological aspects of ceramide.
867   *American journal of physiology. Regulatory, integrative and comparative physiology*
868   290(1):R11-26.
869 67. Shen H*, et al.* (2014) Coupling between endocytosis and sphingosine kinase 1
870   recruitment. *Nat Cell Biol* 16(7):652-662.
871 68. Gnirß K*, et al.* (2012) Cathepsins B and L activate Ebola but not Marburg virus
872   glycoproteins for efficient entry into cell lines and macrophages independent of
873   TMPRSS2 expression. *Virology* 424(1):3-10.
874 69. Bortz RH, 3rd*, et al.* (2020) A Virion-Based Assay for Glycoprotein Thermostability
875   Reveals Key Determinants of Filovirus Entry and Its Inhibition. *J Virol* 94(18): e00336-
876   00320.
877 70. Pfeifer A, Brandon EP, Kootstra N, Gage FH, & Verma IM (2001) Delivery of the Cre
878   recombinase by a self-deleting lentiviral vector: efficient gene targeting in vivo. *Proc
879   Natl Acad Sci U S A* 98(20):11450-11455.
880 71. Griffin BD*, et al.* (2021) SARS-CoV-2 infection and transmission in the North American
881   deer mouse. *Nature Communications* 12(1):3612.
882